JOINT EUROPEAN TORUS JET

JET–P(93)16

J.P. Christiansen, P.M. Stubberfield, J.G. Cordey, C. Gormezano,
C. Gowers, J. O'Rourke, D. Stork, A. Taroni

The Scaling of Transport with Normalised Larmor Radius in JET

The Scaling of Transport with Normalised Larmor Radius in JET

J.P. Christiansen, P.M. Stubberfield, J.G. Cordey, C. Gormezano,
C. Gowers, J. O'Rourke, D. Stork, A. Taroni

JET-Joint Undertaking, Culham Science Centre, OX14 3DB, Abingdon, UK

[1]AEA Industrial Technology, Harwell Laboratory, Oxon, OXll ORA, UK.
[2]University of Birmingham, Birmingham, B15 2TT, UK.

Preprint of a paper to be submitted for publication in Nuclear Fusion
March 1993

ABSTRACT

From first principles of plasma physics the local thermal diffusivity can be expressed in terms of the Bohm diffusivity χ_B and a function F of dimensionless parameters. Tests of transport models, theoretical, empirical or heuristic, expressed in terms of such parameters often produce ambiguous answers which arise from collinearities in the experimental data. In experiments on dimensionally similar discharges [1] the scaling of confinement with one single dimensionless parameter can be examined in a more un-ambiguous fashion. Experiments on JET have been carried out in which only the normalised Larmor radius ρ_* is varied. This is achieved by varying the plasma current, the toroidal field, the density, the ion cyclotron frequency and power level in a predetermined pattern such that other dimensionless parameters like normalised collisionality ν_*, β and safety factor q_ψ are kept constant. The experiments on JET demonstrate that L-mode confinement both globally and locally scales with ρ_* according to the long wavelength or Bohm scaling. The implications for theory and future experiments are outlined.

1. INTRODUCTION

In Tokamak research confinement studies employ three different approaches to determine what governs energy transport: i) in the theoretical approach the emphasis is on the understanding of physics mechanisms which can explain the experimentally observed anomalous loss; ii) the empirical approach with its roots firmly in the experimental Tokamak programme aims at scaling from present data to future machines; iii) a heuristic approach has been adopted by some researchers who combine theoretical features with experimental facts, often for computer simulations of present and future Tokamaks. Each approach has produced a wealth of papers on confinement theories, scaling laws, plasma transport models, etc. It is, however, generally believed that at present no single theory, scaling law or computer simulation is capable of accurately projecting the energy loss rate in a Tokamak reactor plasma from the extensive accretion of data on Tokamaks like JET, DIIID, TFTR, JT60. It has been stressed in [1] and elsewhere, that such a projection involves only an extrapolation of the energy loss rate with respect to one single dimensionless parameter ρ_*, the normalised Larmor radius. Other parameters characterizing a reactor plasma and hence its loss rate, can be held at values of present Tokamaks. An accurate assessment of the dependence of the plasma energy loss rate upon ρ_* is therefore,

experimentally as well as theoretically, a critical issue in Tokamak Research for estimating the performance of a reactor.

The recognition of this issue has led to a series of experiments being carried out on the DIIID Tokamak [1, 2], on TFTR [3, 4] and on JET [5]. On each of these three Tokamaks the experiments have aimed at producing a sequence of discharges which are dimensionally similar [1], but which have different values of the dimensionless parameter ρ_*. This type of confinement study is based on the dimensional analysis by Kadomtsev [6] and Connor-Taylor [7]. Scale invariance arguments are applied to several possible forms of transport equations (Vlasov, MHD etc.) and dimensionally correct forms for thermal diffusivities and power loss rates are obtained. The latter we express via the thermal flux q which may contain several components, diffusive and non-diffusive. The non-diffusive parts q_{flow} are found to be small, i.e. $|q_{flow}| << |q|$, in off-axis heating experiments on JET [8] and DIIID [9]. The diffusive parts q_e (electron loss channel) and q_i (ion loss channel) are combined into the following representation for the total thermal flux.

$$q = - e (n_e \nabla T_e + n_i \nabla T_i) \chi \qquad (1)$$

The effective diffusivity $\chi \equiv \chi_{eff}$ can be associated with either of or both the loss channels. The question addressed by the JET experiments (as well as those on DIIID and TFTR) is: how does q in Eq. (1) depend on dimensionless parameters such as ρ_*?

In Section 2. we define a set of dimensionless parameters and we define q in terms of these parameters. The experiments carried out on JET are described in Section 3 together with the results from an analysis of global JET data. In section 4 we present the main result of the paper; this is based on a series of local transport calculations with the TRANSP code [10]; the results include details of the intended matching of profiles in the experiments together with a few unintended-unavoidable departures from ideal conditions. In the summary section we discuss the implications of our results in the light of those obtained on DIIID [2], TFTR [4, 5] and the joint JET-DIIID similarity experiments [11].

In this paper we use a standard plasma physics notation for plasma parameters and if dimensional, these are expressed in SI units with temperatures in eV.

2. DIMENSIONLESS PARAMETERS

In the scale invariance approach to confinement scaling [7] the scaling of the heat flux q with plasma parameters depends on the choice of physics model. The simplest plasma physics model one can envisage is described by the collisionless Vlasov equation in the electrostatic limit. For this simple model one obtains [7]

$$\chi = \chi_B \, F(\rho_*, \text{"geometry"}) \quad , \quad \chi_B = T/B \tag{2}$$

in which χ_B is the Bohm diffusivity and F is some function of the normalised Larmor radius ρ_* and T, B represent temperature, magnetic field; "geometry" means dimensionless parameters characterizing the plasma geometry, e.g. elongation. To cover more complex models which include the physics of collisions, plasma equilibrium, instabilities etc., this simple representation must be replaced by

$$\chi = \chi_B \, F(\rho_*, p_1, p_2, \ldots) \tag{3}$$

in which p_j denotes a set of dimensionless parameters describing various aspects of plasma physics. By combining χ_B and p_j other formal representations are possible and the review by Connor [12] describes many of these.

The representation (3) is thus completely general provided the parameters p_j form a complete set of physics parameters relevant for thermal transport. Such a complete set would, however, be too untractable in analyses of experimental data for two reasons: i) empirical results show some parameters to be irrelevant for confinement physics; ii) some parameters cannot be estimated or inferred accurately from experimental measurements. Parameters describing atomic and radiation physics and parameters based on length-time scales of order Debye lengths-inverse plasma frequency can be discarded; one reason for this omission is that global confinement data in the ITER data bases has been demonstrated [13] to satisfy the so-called Kadomtsev constraint; this constraint [6] implies that F in (3) does not depend on λ_D, the Debye length.

Reduced sets p_j of dimensionless parameter definitions can be found in the literature: ref. [3] defines 18, ref. [12] treats 6, ref. [14] uses 10 etc. The set considered in this paper is defined below and B denotes the poloidal field while B_ϕ is the toroidal field.

The plasma surface geometry is characterised by

aspect ratio $\varepsilon = ax/R_o$, ellipticity E and triangularity Δ.

The scale lengths of n, T, safety factor as well as, shear and power deposition profiles are

$$\varepsilon_n^{-1} = R_o < \nabla n > /n \quad , \qquad \varepsilon_T^{-1} = R_o < \nabla T > /T$$

$$q_\psi = \frac{RB_\phi}{2\pi} \oint \frac{d\ell}{R^2 B} \approx \varepsilon E^{1/2} < B_\phi / B > \quad , \quad s = x q'/q \tag{4}$$

$$g_p = P(x)/P = \frac{1}{P} \int_o^x q(x) \frac{1}{a} V' \, dx;$$

Ratios for species are expressed via

$$Z_{eff}, \quad T_e/T_i, \quad m_P/m_e, \quad M = m_i/m_P.$$

The three dimensionless parameters describing FLR, collisions and pressure are

$$\rho_* = \left(\frac{m_P}{e}\right)^{1/2} \frac{M^{1/2} T_e^{1/2}}{aB}; \quad \nu_* = \left(\frac{e^2 \log \Lambda}{3(2\pi)^{3/2} \varepsilon_o^2}\right) \frac{naZ_{eff}}{T_e^2}; \quad \beta = (4e\mu_o) \frac{n_e T_e + n_i T_i}{2B^2} \tag{5}$$

We notice that the local dimensionless parameters are defined in terms of local variables and one characteristic global length scale, minor radius a. By doing so we follow other authors although in principle the minor radius a could be replaced by a local measure such as $L_n = n/\nabla n$.

In similarity scaling experiments [1] attempts are made to vary only one dimensionless parameter while keeping the remainder of the set fixed. Since in experiments we can only control a, n, B, T (or P) we form the inverse relations using a one fluid treatment with $n_e = n_i = n$ and $T_e = T_i = T$; the bracketed terms of Eq. (5) C_ρ, C_ν, C_β combine to various forms like $C_\rho{}^x C_\nu{}^y C_\beta{}^z$ which for brevity we label e.g. C_B

$$B = C_B \; a^{-5/4} \; \rho_*^{-3/2} \; \nu_*^{-1/4} \; \beta^{1/4} \; M^{3/4} \; Z_{eff}^{1/4}$$

$$T = C_T \; a^{-1/2} \; \rho_*^{-1} \; \nu_*^{-1/2} \; \beta^{1/2} \; M^{1/2} \; Z_{eff}^{1/2} \tag{6}$$

$$n = C_n \; a^{-2} \; \rho_*^{-2} \; \beta \; M$$

$$\chi_B = C_\chi \; a^{3/4} \; \rho_*^{1/2} \; \nu_*^{-1/4} \; \beta^{1/4} \; M^{-1/4} \; Z_{eff}^{1/4}$$

Eqs. (6) show the scaling of plasma variable with minor radius a and the dimensionless parameters. The total power input P scales as ~n Ta χ_B F or

$$P = C_P \; a^{-3/4} \; \rho_*^{-5/2} \; \nu_*^{-3/4} \; \beta^{7/4} \; M^{5/4} \; Z^{3/4} \; F \qquad (7)$$

while the fusion product scales as

$$nT\tau_E = C_F \; a^{-5/4} \; \rho_*^{-7/2} \; \nu_*^{-1/4} \; \beta^{5/4} \; M^{7/4} \; Z^{1/4} \; F^{-1}$$

In the similarity experiments on JET the scanning of ρ_* at constant ν_*, β, q_ψ etc. implies from Eq. (6) that $n \sim B^{4/3} a^{-1/3}$, $T \sim B^{2/3} a^{1/3}$, $B \sim I_\phi \sim B_\phi$. From Eq. (6) we can derive global averages, denoted by angular brackets, such as those used in [13] $<\rho_*>$, $<\nu_*>$, $<\beta>$ etc. Eq. (7) thus determines the power level required to establish dimensionally similar discharges once a variation of F with ρ_* is assumed; conversely $F(\rho_*)$ can be determined using Eq. (7) from the power levels at various B (or I_ϕ) required for matching the values of ν_* and β. Three generic plasma models (F_0 is some number) are described by

$$F = F_0 \, \rho_*^{x_\rho} \qquad (8)$$

The value of the exponent x_ρ indicates a characteristic length scale λ associated with turbulent transport: for $x_\rho = -1$ one has $\lambda >> a$, corresponding to a plasma with ergodic field lines; for $x_\rho = 0$ $\lambda \sim a$ corresponding to long wavelength turbulence and the scaling (8) is the Bohm scaling; for $x_\rho = 1$ $\lambda \sim \rho_s$ in which case the transport arises from short wavelength (Larmor radius) turbulence and the scaling (8) is then referred to as gyro-reduced Bohm or gyroBohm scaling which is common to most theoretical models [3, 12]. By inserting Eq. (8) in Eq. (7) and using Eq. (6) to substitute B for ρ_* we find that the power input scaling required to match the three generic plasma models $x_\rho = -1, 0, 1$ becomes

$$P(x_\rho = -1) \sim I_\phi^{7/3}, \qquad P(x_\rho = 0) \sim I_\phi^{5/3}, \qquad P(x_\rho = 1) \sim I_\phi \qquad (9)$$

The purpose of the JET experiments described in the next section is essentially to determine x_ρ. In terms of the global parameters in (9) we notice that if I_ϕ is increased by e.g. a factor 2 at constant ν_*, β, q_ψ, the input power required should be increased by a factor 5.04, 3.17, 2 respectively.

3. JET SIMILARITY EXPERIMENTS

In the JET experiments ICRH has been used as the additional heating method in preference to NBI; since density n must vary in a scan of ρ_* the use of NBI can lead to different heating profiles [1-4]. The available range of ω_{ICRH} on JET is 27-55 Mhz and thus a range by a factor 2 in B_ϕ is possible with on-axis heating. A series of 3 different Tokamak discharges with I_ϕ = 2, 3, 4 MA, B_ϕ = 1.7, 2.6, 3.4, ω_{ICRH} = 27, 41, 54 Mhz all have κ = 1.44, q_ψ = 4.37, a = 1.18 and density varies as n ~ $B_\phi^{4/3}$ or $I_\phi^{4/3}$. This ensures globally (see Eq. 6) that

$$< \nu_* > \; < \beta >^2 = \text{const} \tag{10}$$

The ICRH power has been varied from 2.7 to 14 MW to cover the range predicted by Eq. (9) for I_ϕ = 2, 3, 4 MA; fine tuning of P at the upper and lower ends of the range has resulted in 7 2MA, 4 3MA and 5 4MA discharges. The global data from these discharges depicting the relation (10) is shown in Fig. 1. The 2, 3, 4 MA pulses are represented by circles, triangles and squares respectively. It can be seen that the path of Eq. (10) is represented very well by the data. The arrow in Fig. 1 points to the three most similar pulses. These three pulses # 27658 (2 MA), # 27680 (3 MA), # 27654 (4 MA) will be the subject of a detailed local analysis in the next section.

The global confinement scaling can be examined by studying the variation of $\tau_E / (\tau_B <F>)$ with $<\rho_*>$; the Bohm time is $\tau_B = \frac{3}{4} a^2 / <\chi_B> = \frac{9}{4} e\mu_o \pi a^2 <n> I_\phi \kappa / \varepsilon P \tau_E$ and <F> is given by Eq. (8). In Fig. 2 we show for x_ρ = - 1, 0, 1 the ratio $\tau_E / \tau_B <F>$ vs $<\rho_*>$ for all 16 pulses. This ratio should for the correct scaling approximately be equal to some constant; despite the slight variations in ν_* and β (see Fig. 1) it can clearly be seen from Fig. 2 that the Bohm scaling x_ρ = 0 is the best representation of the data; the three lines in Fig. 2 are the result of linear regression fits to the data points. This result is also immediately recognised from the power input requirements of Eq. (9).

The three most similar pulses arrowed in Fig. 1 have P = 4.1, 8.1, 12.0 MW respectively close to the Bohm scaling ratios of 1, 1.97, 3.17. Thus global confinement in the JET similarity experiments exhibits the long wavelength or Bohm scaling characteristic of L-mode plasmas. That same result has been found in the similarity experiments on DIIID [1, 2] and on TFTR [3, 4]. Analysis of global confinement with the ITER L-mode database [13] has also produced this result.

4. THE SCALING OF LOCAL HEAT FLOW

A series of local transport calculations with the TRANSP code [10] have been carried out for the three pulses indicated by an arrow in Fig. 1. We shall present results for the 2 and 4 MA pulses for which the $<\rho_*>$ ratio ~ $B^{2/3}$ is 1.59. The heat deposition profiles for ions and electrons $Q_{ICRHe,i}$ (x) due to minority ions accelerated by ICRF is calculated by the SPRUCE code [15]. No charge-exchange ion temperature profile data is available since ICRH is used rather than NBI. The calculations employ a Kadomtsev model for flattening the q profile inside the inversion radius following a sawtooth crash; the inversion radius at R = 3.6 m inferred from ECE measurements in all three pulses agrees with that measured by the Faraday rotation measurements; it corresponds to x = 0.4 and is between the values 0.29 quoted for TFTR [4] and 0.5 for DIIID [16]. At a sawtooth crash no changes to the heat deposition profiles $Q_{ICRHe,i}$ (x) are made to describe the redistribution of energetic minority ions; such changes are however estimated to be negligible as most of the ICRF power is deposited inside x = 0.3. The TRANSP calculations use as input diagnostic data on $T_e(x)$, $n_e(x)$, T_{io}, Z_{eff}, P together with the plasma boundary determined from fits to magnetic pick-up coil data. The output data values include $n_i(x)$, $T_i(x)$, q(x), B(x), $B_\phi(x)$. This data has been selected from those calculations which best reproduce the diagnostic data (global confinement time, loop voltage, Faraday rotation) that is not used as input. Two models for χ_i have been considered. The first model with $\chi_e = \chi_i$ cannot reproduce the X-ray crystal spectrometer data on T_{io}. In the second model, which has been used for our analysis, $\chi_i = \alpha\chi_{neoclass.}$ where α is determined from the T_{io} data. The calculated T_i profile is not used directly for our conclusions but only to monitor the T_e/T_i ratio.

The output data from TRANSP calculations exhibits time variations due to sawteeth and due to variations in the measured input data. This is particularly noticeable for the collisionality ν_*. In Figs. 3a-3d we show the global averages of $<\rho_*>$, $<\nu_*>$, $<\beta>$ and $q_\psi(x=1)$ vs time. The data values in the time window of 1.6

s indicated by arrows, are smoothed by a running average method at each radial point $0.375 \leq x \leq 0.875$.

The profiles from which we draw our inferences about the scaling of local heat flux are shown in Figs. 4a-4d. From such profiles we form the ratio between the 4 MA and the 2 MA data of the dimensionless parameters given by Eqs. (4-5) and these ratios are plotted in Figs. 5a-5h. It can be seen that the profiles for the 4 and 2 MA pulses are very well matched; only the ε_n and ε_T ratios, Figs. 5g and 5h, show systematic departures from 1. From the error bars in Fig. 5f showing the magnetic shear ratio, the effects of sawteeth can be seen on the first two radial points.

For dimensionally similar pulses the thermal flux can then be normalised as

$$q_* = q/q_{model} \quad , \quad q_{model} = - en\, \chi_B\, F_{model}\, \frac{T}{a}$$

The surface averaged gradient ∇T ($T = T_e$) has been replaced by T/a, because T is more accurately measured than ∇T. Those models, for which the ratio q_{*2} / q_{*1} between discharges 2 and 1 is closest to 1, have the best prescription of the variation of F with the scanned parameter ρ_*. This technique offers an unambiguous test of transport models since

$$\frac{q_{*2}}{q_{*1}} = \left(\frac{a_2\, q_2\, B_2}{a_1\, q_1\, B_1} \; \frac{n_1\, T_1^2}{n_2\, T_2^2} \right) \frac{F_{model}\ (\rho_{*1})}{F_{model}\ (\rho_{*2})} \qquad (11)$$

The bracketed term should be a constant C_o across the radius x; the F_{model} ratio too should be a constant $1/C_o$ if the model is right. Experimental imperfections or unintended mismatches between discharges 1 and 2 can be assessed via the bracketed term; its departure from C_o implies that the set p_j is not perfectly matched.

The main result of this paper is demonstrated in Fig. 6. Ratios of the normalised heat flow (Eq. 11) are shown against radius for the model $F = F_o\, \rho_*^{x_\rho}$, which the experiments aim at testing. From the three choices $x_\rho = -1$ (MHD), $x_\rho = 0$ (Bohm), $x_\rho = 1$ (gyroBohm) in Fig. 6 it can clearly be seen for $x_\rho = 0$ (Bohm) that the ratio is remarkably constant and equal to 1 across the radius; Fig. 6 presents locally what Fig. 2 does globally: the same symbols for the three choices of x_ρ are used and the two sets of variations with ρ_* are fully consistent. It can now be argued on the

basis of Figs. 5a-5h that we have not kept all the dimensionless parameters absolutely constant in the experiments. We can therefore test theoretical and empirical models which predict dependencies of F additional to that upon ρ_*; such models are listed in the Appendix. Figs. 7a-7d show the ratios (Eq. 13) for four gyroBohm based models which also depend on ν_*, β, q_ψ, s etc.; Figs. 8a-8d similarly show ratios for two empirical and two resistive MHD scalings. The pure resistive MHD scaling ~ S^0 (S is Lundquist number) is gyroBohm like (Fig. 8c); a model which assumes F ~ $S^{1/2}$ becomes Bohm-like but it reflects (Fig. 8d) too strong a variation with ν_*. (Note that the axis ranges in Figs. 6-8 differ but in all cases cover a factor 4). The vertical bars in Figs. 5a-5d represent the variances σ_p of a parameter p while the symbols denote the mean of p according to

$$p = \bar{p} + \sigma_p$$

The evaluation is performed by a statistics programme package which assumes a Gaussian distribution of N time values $p(t_k)$, k = 1, N; typically 50 < N < 70. For the flux ratios (Eq. 11) shown in Figs. 6-8, the vertical bars are representative of the Gaussian estimate

$$q_{*2} / q_{*1} = \bar{q}_{*2} / \bar{q}_{*1} \left(1 + \left(\delta q_{*1}^2 + \delta q_{*2}^2\right)^{1/2}\right) \qquad (12)$$

where the normalised variance is $\delta q_1 = \sigma_{q_1} / \bar{q}_{*1}$. Eq. (12) expresses the range of variation in the values of q_* calculated by the TRANSP code, i.e. the L.H.S. of Eq. (11). It is different from the range of q_* which can be expected from the experimental measurement errors. Because we are looking for a systematic trend w.r.t. ρ_* of Eq. (11) we can estimate the variation of the R.H.S. of Eq. (11) by adding the errors in a Gaussian sense of n, T, q, B, F. This yields

$$\Delta(q_{*2} / q_{*1}) = \sqrt{2}\left(\delta q^2 + \delta B^2 + \delta n^2 + 2\delta T^2 + \delta F^2\right)^{1/2} \qquad (13)$$

This estimate does not of course include errors which are common to all the similarity pulses, e.g. systematic calibration errors. The pure Bohm scaling has $\delta F = 0$ and yields the smallest error estimate; because q_ψ is well matched we set

$\delta B = \delta B_\phi \approx 0$ and assume $\delta q = \delta n = \delta T$. Since the ρ_* ratio (see Figs. 5a and 6) is 1.6 we see from Eq. (13) that a relative error of order $0.6/2\sqrt{2} = 0.21$ is required to change the conclusions made in Fig. 6; this error must be present in q, in n, and in T across the radius x for both the 2 MA and the 4 MA discharges. For the JET diagnostics the errors δq, δn, δT are functions of radius x: δT is smallest in the centre and largest at the edge (ECE diagnostic); δq is largest in the centre and vanishes at the edge; δn is approximately constant until $x = 0.85$ and then rises sharply. Thus a change of the trend with ρ_* established in Fig. 6, arising from experimental measurement errors, does not seem very likely.

If a gyroBohm or ideal MHD based model has to be accommodated by the JET data then the only possibility lies in having F a function of ε_n or ε_T or both (see Figs. 5a-5h). Such a function could be

$$F = \rho_*^{\pm 1} \quad \varepsilon_T^{x_T} \quad \varepsilon_n^{x_n}$$

From Figs. 5g and 5h we notice that the ε_n, ε_T ratios are ~ 1.1 and 0.9 respectively. This would imply that $(x_T, x_n) \approx (-3, 3)$ or $(3, -3)$ for the gyroBohm or MHD scalings respectively or alternatively $x_n = 0$, $x_T = \pm 6$. Presently no theory has predicted such a strong dependence.

5. SUMMARY

The main result from the JET similarity experiments is that the heat flux in the bulk of L-mode plasmas locally exhibits the Bohm or long wavelength scaling $\chi = \chi_B F_o$; this result is fully consistent with the global scaling result of section 4 and with global scaling laws such as [13, 22, 23]. Other models based on the MHD and gyroBohm scalings of confinement with ρ_* have been tested but they do not give a good fit to the data. The dimensionless parameters in Fig. 5 have not been held absolutely constant, but the JET data cannot easily accommodate an MHD or gyroBohm based scaling even when allowances for the experimental imperfections are made.

The testing of transport models against experimental global and local confinement data is in general difficult. We believe, however, that the JET similarity experiments, scanning ρ_* with a variation of a factor of 1.6, have conclusively shown that global and local transport in limiter L-mode plasmas exhibit the scaling with ρ_* characteristic of long wavelength turbulence or Bohm;

that same result has been obtained on TFTR [3, 4] and to some extent on DIIID [2]. The implications of the scaling of confinement with ρ_* for extrapolations to a reactor are important: gyroBohm based theories with $x_\rho = 1$ are optimistic extrapolations while MHD scalings with $x_\rho = -1$ are pessimistic; the Bohm scaling with $x_\rho = 0$ exhibits a trend between the former two and as mentioned, is embodied in empirical scaling laws. Future similarity experiments can examine the scaling in X-point configuration plasmas with L, H or VH mode confinement characteristics.

ACKNOWLEDGEMENTS

The authors acknowledge members of the JET team for making the experimental data available.

Appendix : Transport Models

We list a number of theoretical, empirical and heuristic transport models for the diffusivity χ as represented by Eq. (3) (see also [12]). If a transport model gives only an expression for τ_E then the F function is derived from global averages. References are given and possible residual dependencies of F as well as numerical constants are omitted.

1.	Electrostatic Vlasov or pure Bohm [7]			$F = F_o$
2.	Short wavelength or pure gyroBohm [1-5]			$F = \rho_*$
3.	Ideal MHD [14]			$F = \rho_*^{-1}\, \beta^{-1/2}$
4a.	Resistive MHD,	S^o	[12]	$F = \rho_*\, \nu_*\, \beta^{-1}$
4b.		$S^{-1/2}$		$F = \rho_*^2\, \nu_*^{3/2}\, \beta^{-5/4}$
4c.		$S^{1/2}$		$F = \nu_*^{1/2}\, \beta^{-3/4}$
4d.		S^1	[17]	$F = \rho_*^{-1}\, \beta^{-1/2}$
5.	η_i modes [18]			$F = \rho_*\, s^{-1}\, \varepsilon_n\, (T_e/T_i)^{-1}\, (\eta_i - 2/3)^{1/2}$
6.	DTIM [19]			$F = \rho_*\, \nu_*^{-1}\, s^{-2}\, \varepsilon_n^{-1}\, q_\psi^{-1}\, \varepsilon^{1/2}\, M^{-1/2}$
7.	Drift waves [20]			$F = \rho_*\, s^{-1}\, \varepsilon_n^2\, \varepsilon^2\, (\nu_*\, q_\psi)^{0 \text{ or } 1}$
8.	Resistive fluid Turbulence [12]			$F = \rho_*\, \nu_*\, \beta^{-1/2}\, M^{-1/2}$
9.	Rebut-Lallia-Watkins		[21]	$F = \rho_*\, \nu_*^{1/2},\, \beta^{-1/2}\, (1-\varepsilon)\, s^{-1}\, q_\psi\, \varepsilon\, (\varepsilon_T^{-1} + 2\, \varepsilon_n^{-1})\, (T_e/T_i)^{1/2}\, M^{1/2}\, (1+Z_{eff})^{1/2}$
10.	ITER L-thermal [13]			$F = \nu_*^{0.15}\, \beta^{1.21}$

11. Goldston [22] $F = (ax)^{0.26}\,\beta/\chi_B$
    The nearest dimensionally correct form is $F = \rho_*^{0.18}\,\nu_*^{0.34}\,\beta^{0.36}$

12. ITER89P [23] $F = \rho_*^{0.08}\,\nu_*^{0.25}\,\beta^{0.28}$

The Lundquist number $S = \rho_*^{-2}\,\nu_*^{-1}\,\beta^{1/2}$ is used to produce various resistive MHD scalings. The model 9 features an additional critical gradient term [3, 21]. The empirical scaling laws 11 and 12 have been transformed to dimensionally correct forms by adjusting the exponents of the scaling law as follows: Goldston $\delta_n = \delta_I = \delta_P = -\delta_a = 0.052$ and ITER89P $\delta_n = \delta_I = \delta_P = -\delta_a = 0.048$.

REFERENCES

[1] WALTZ, R.E., DEBOO, J.C., ROSENBLUTH, M.N., Phys. Rev. Lett. 65 (1990) 2390.

[2] WALTZ, R.E., DEBOO, J.C., OSBORNE, T.H., Nucl. Fusion 32 (1992) 1051.

[3] PERKINS, F.W., BARNES, C.W., JOHNSON, D.W., SCOTT, S.D., et al., Nondimensional Transport Scaling in the Tokamak Test Fusion Reactor: Is Tokamak Transport Bohm or GyroBohm?, to appear in Phys. Fluids.

[4] SCOTT, S.D., BARNES, C.W., MIKKELSEN, D.R., PERKINS, F.W., in Plasma Physics Controlled Nuclear Fusion Research, 1992, 14th Int. Conf. Wurzburg, Paper IAEA-CN-56/G-3-3.
JOHNSON, P., TTF Workshop, PPPL (1990) ρ_* and ν_* scans on TFTR.

[5] CHRISTIANSEN, J.P. BALET, B., BOUCHER, D., CHALLIS, C., et al., Evidence for a local diffusive model of Transporting a Tokamak, 19th EPS Conference, Innsbruck 1992. Plasma Physics and Controlled Fusion 34 (1992) 1881

[6] KADOMTSEV, B.B., Sov. J. Plasma Physics 1 (1975) 295.

[7] CONNOR, J.W., TAYLOR, J.B., Nucl. Fusion 17 (1988) 1047.

[8] BALET, B., CORDEY, J.G., MUIR, D.G., SCHMIDT, G.L., Nucl. Fusion 32 (1992) 1261.

[9] LUCE, T., PETTY, C.C., SCHISSEL, D.P., DEBOO, J.C., Phys. Rev. Lett. 62 (1992) 51.

[10] HAWRYLUK, R.J., An empirical approach to Tokamak Transport, Proc. Course and Workshop 1979, Vol. 1, p. 19,
Rep. EUR-FU-BRU/XII/476/80, CEC, Brussels (1980)
GOLDSTON, R.J., J. Comp. Phys. 43 (1981) 61.

[11] CARLSTROM, T.N., CHRISTIANSEN, J.P., DEBOO, J.C., WALTZ, R.E., ρ_* scaling of Confirment in Dimensionally similar discharges in JET and DIIID, 34th APS Meeting Seattle (1992), 3E5, page 1410, Bulletin of the American Physical Society Vol. 37, No. 6, November 1992.

[12] CONNOR, J.W., Plasma Physics Contr. Fusion 20 (1988) 619.

[13] CHRISTIANSEN, J.P., CORDEY, J.G., KARDAUN, O.J.W.F., THOMSEN, K., Nucl. Fusion 31 (1991) 2117.

[14] BICKERTON, R.J., Indications from Dimensional Analysis of the L-mode Database, Rep. FRCR 374, Texas Univ., Austin (1990).

[15] SMITHE, D.N., et al., Nucl. Fusion 27 (1987) 1319.

[16] SNIDER, R., Nucl. Fusion 30 (1990) 2400.

[17] THOMAS, P.R., A Comparison Between Additional Heating Data and Forms with Model Scale Invariance. Preprint JET P (87) 17, JET Joint Undertaking (1987).

[18] HONG, B.G., HORTON, W., Phys. Fluids B2 (1990) 979.

[19] DIAMOND, P.H., BIGLARI, H., Phys. Rev. Lett. 65 (1990) 2865.

[20] WALTZ, R.E., DOMINGUEZ, R.R., WONG, S.K., et al., in Plasma Physics and Controlled Nuclear Fusion Research 1986 (Proc. 11th Int. Conf. Kyoto, 1986), Vol. 1, IAEA, Vienna (1987) 345.

[21] REBUT, P.H., LALLIA, P.P., WATKINS, M.L., in Plasma Physics and Controlled Nuclear Fusion Research 1988 (Proc. 12th Int. Conf. Nice 1988), Vol. 2, IAEA, Vienna (1989) 191.

[22] GOLDSTON, R.J., Plasma Physics Contr. Fusion 26 (1984) 27.

[23] YUSHMANOV, P.N., TAKIZUKA, T., RIEDEL, K.S., et al., Nucl. Fusion 30 (1990) 1999.

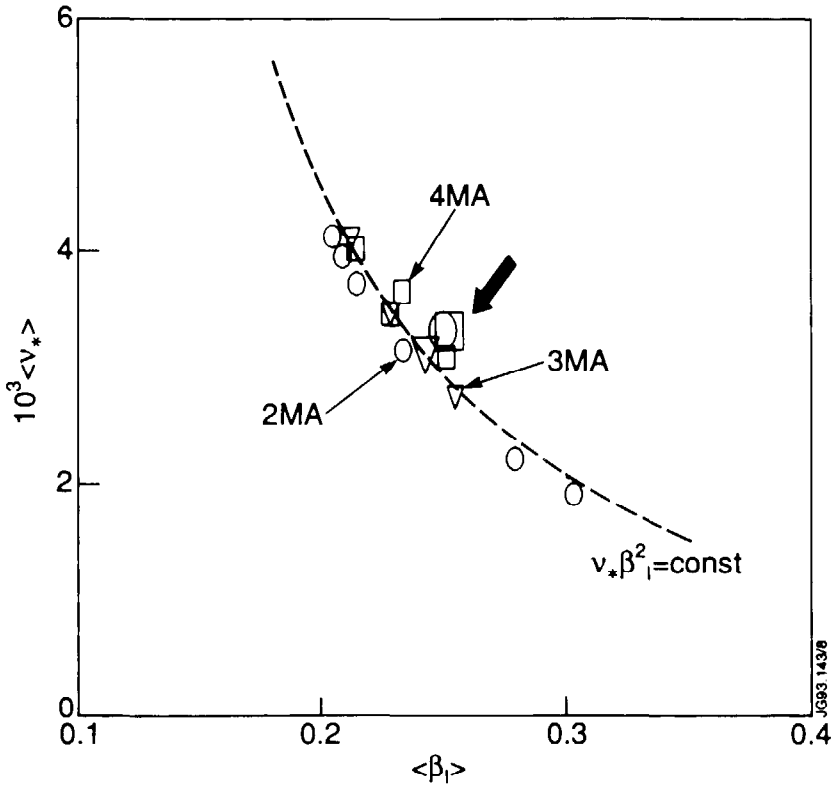

Fig. 1: The global averages for 16 pulses of $<\nu_*>$ vs. $<\beta>$. Circles, triangles and squares refer to 2, 3, 4 MA pulses. The three pulses 27654, 27658, 27680 chosen for analysis are shown by larger symbols and an arrow.

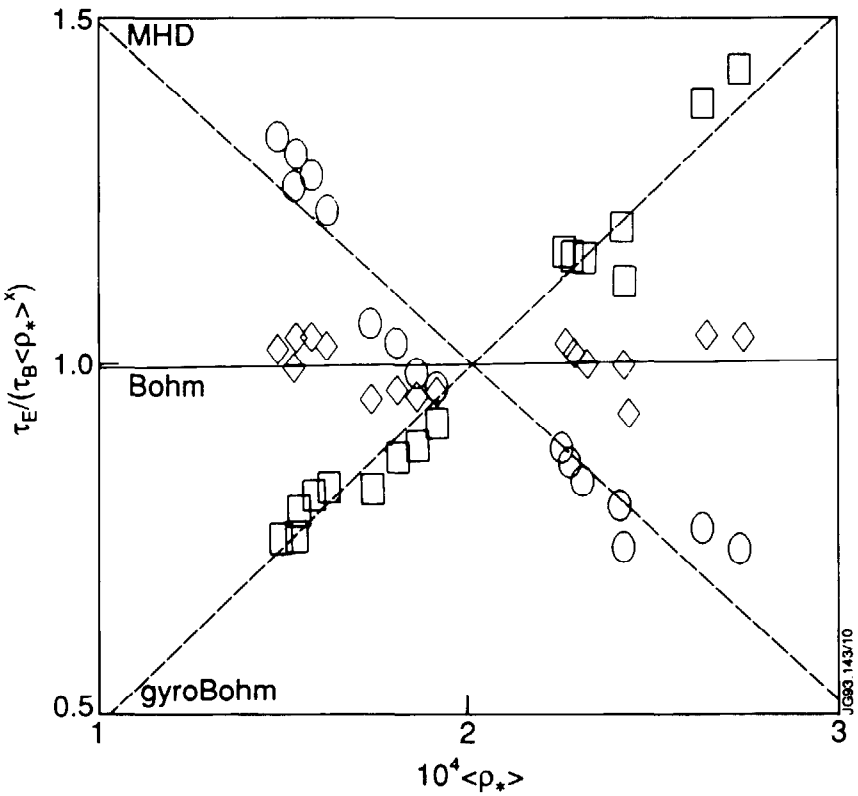

Fig. 2: The ratio τ_E/τ_B <F> for the 16 "almost" similar pulses plotted against $<\rho_*>$. The square symbols correspond to (see Eq. 7a) x_ρ = 1 (gyroBohm), diamonds are for x_ρ = 0 (Bohm) and circles are for x_ρ = -1 (Ideal MHD).

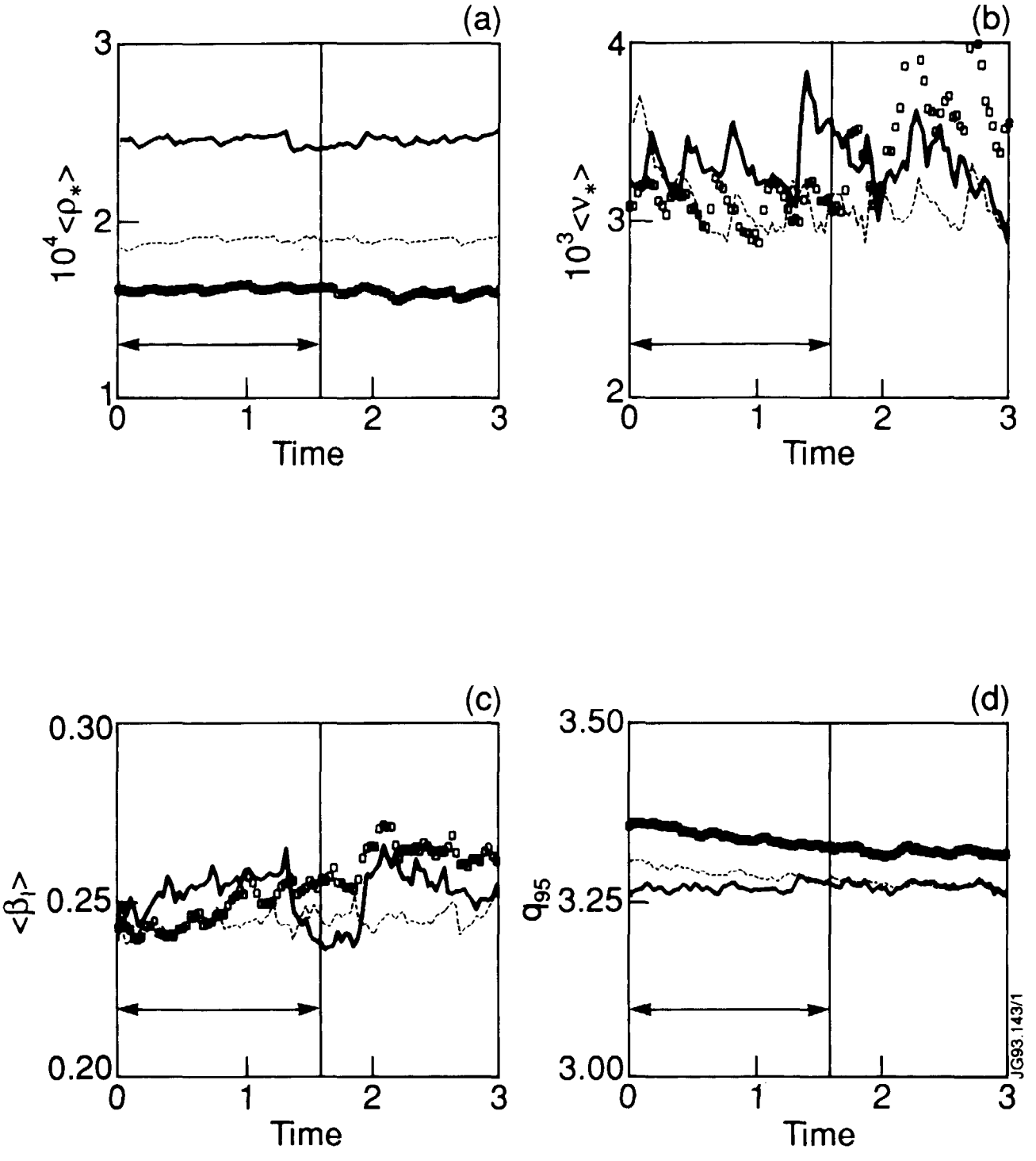

Fig. 3: Time variation of (a) $\langle \rho_* \rangle$, (b) $\langle \nu_* \rangle$, (c) $\langle \beta \rangle$, (d) q_ψ for the three pulses arrowed in Fig. 1. The time interval chosen for analysis is marked. Full line, square symbols, dashed line refer to the three selected pulses.

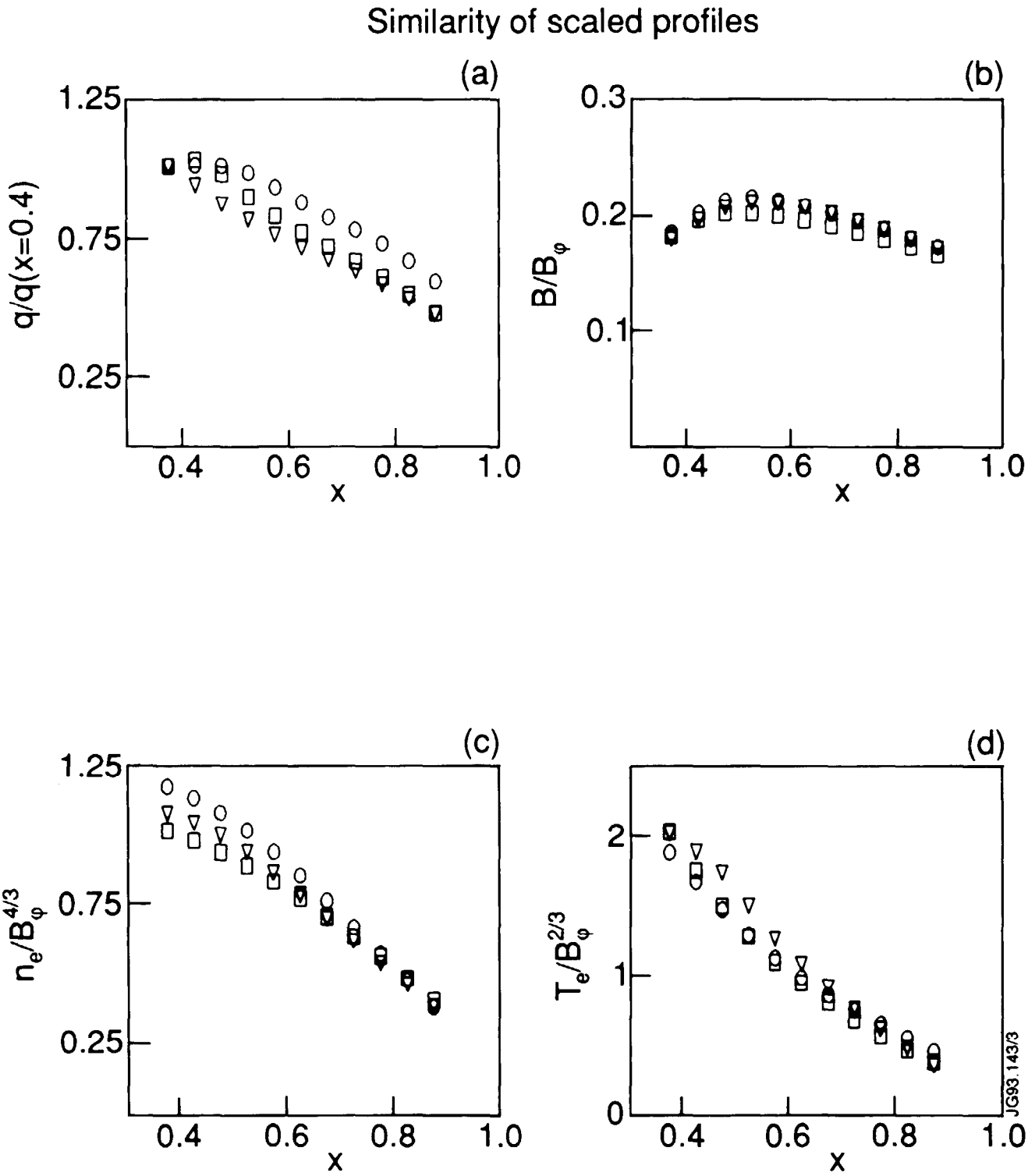

Fig. 4: Time averaged spatial profiles of heat flux q (a), poloidal field B (b), density (c), temperature (d).

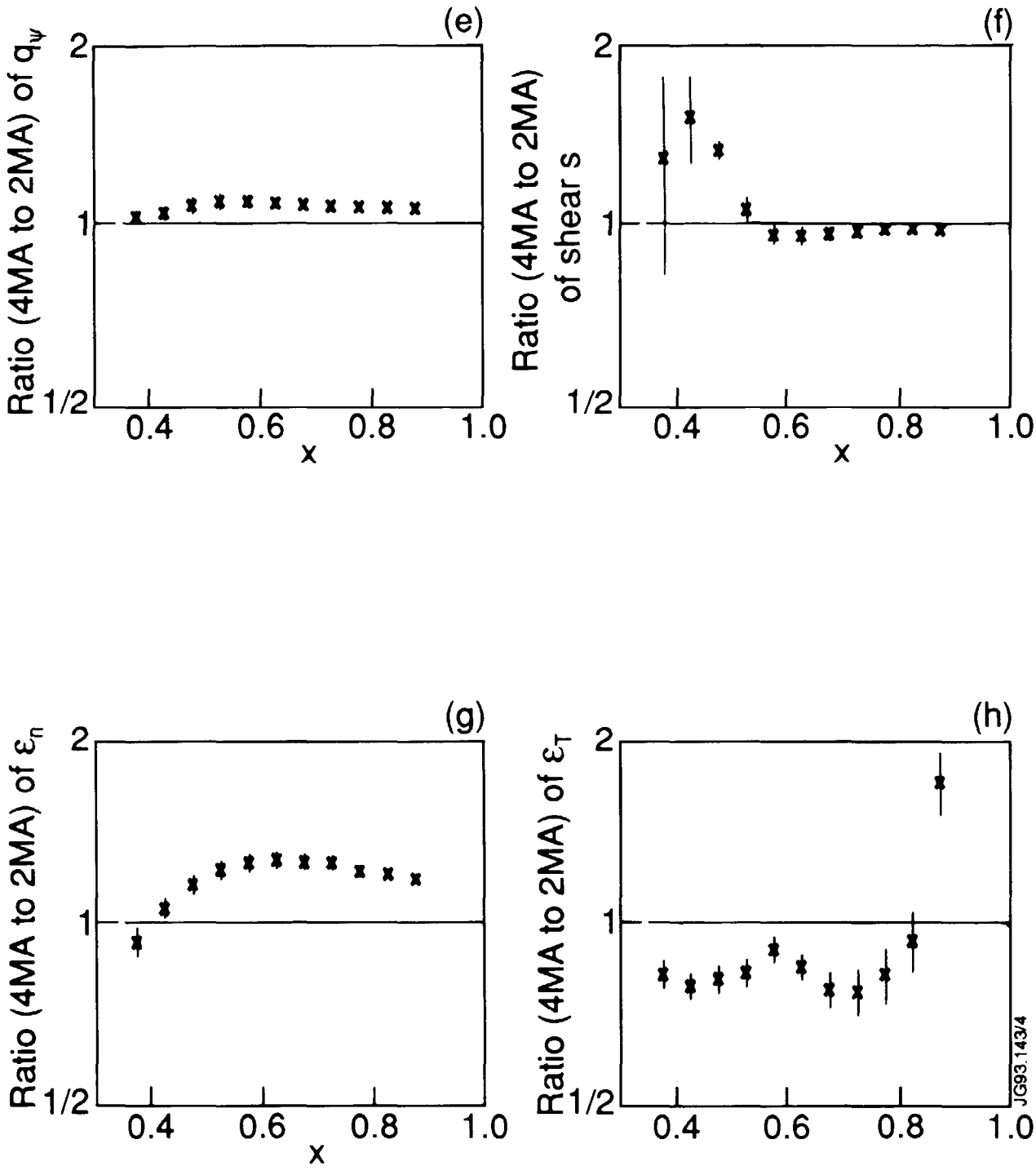

Fig. 5: The time averaged 4 to 2 MA ratios of (a) ρ_*, (b) ν_*, (c) β, (d) T_e/T_i, (e) q_ψ, (f) s, (g) ε_n, (h) ε_T. The definitions of these local parameters are given in Eqs. (4-5). Vertical bars indicate variances (see text).

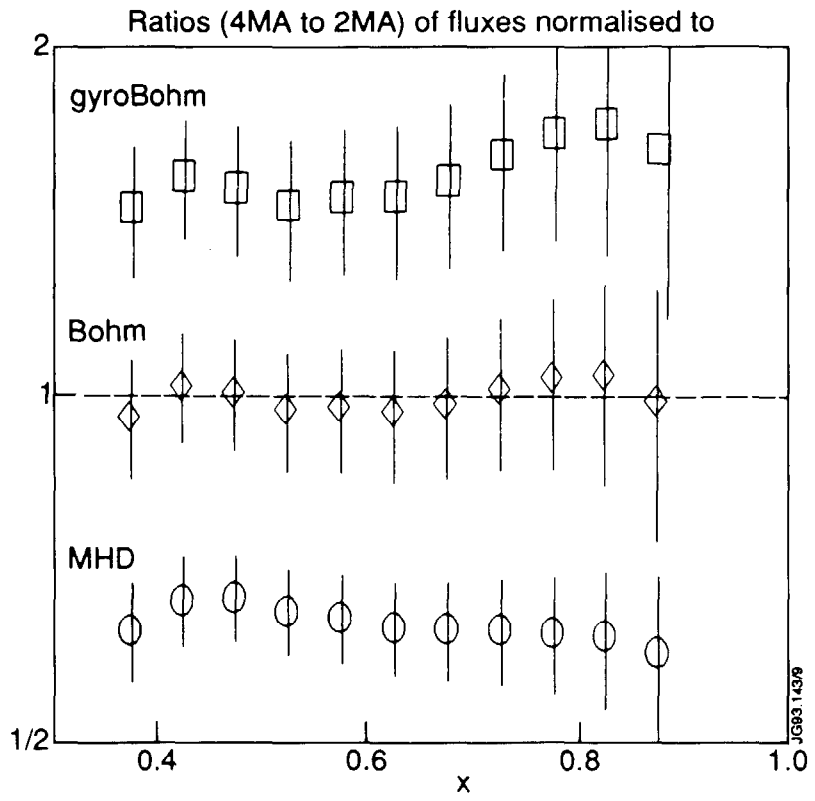

Fig. 6: The 4 to 2 MA ratio of normalised thermal fluxes (Eq. 11) with $F = F_o \rho_*^{x_\rho}$ for x_ρ = - 1, 0, + 1, corresponding to MHD, Bohm and gyroBohm scalings.

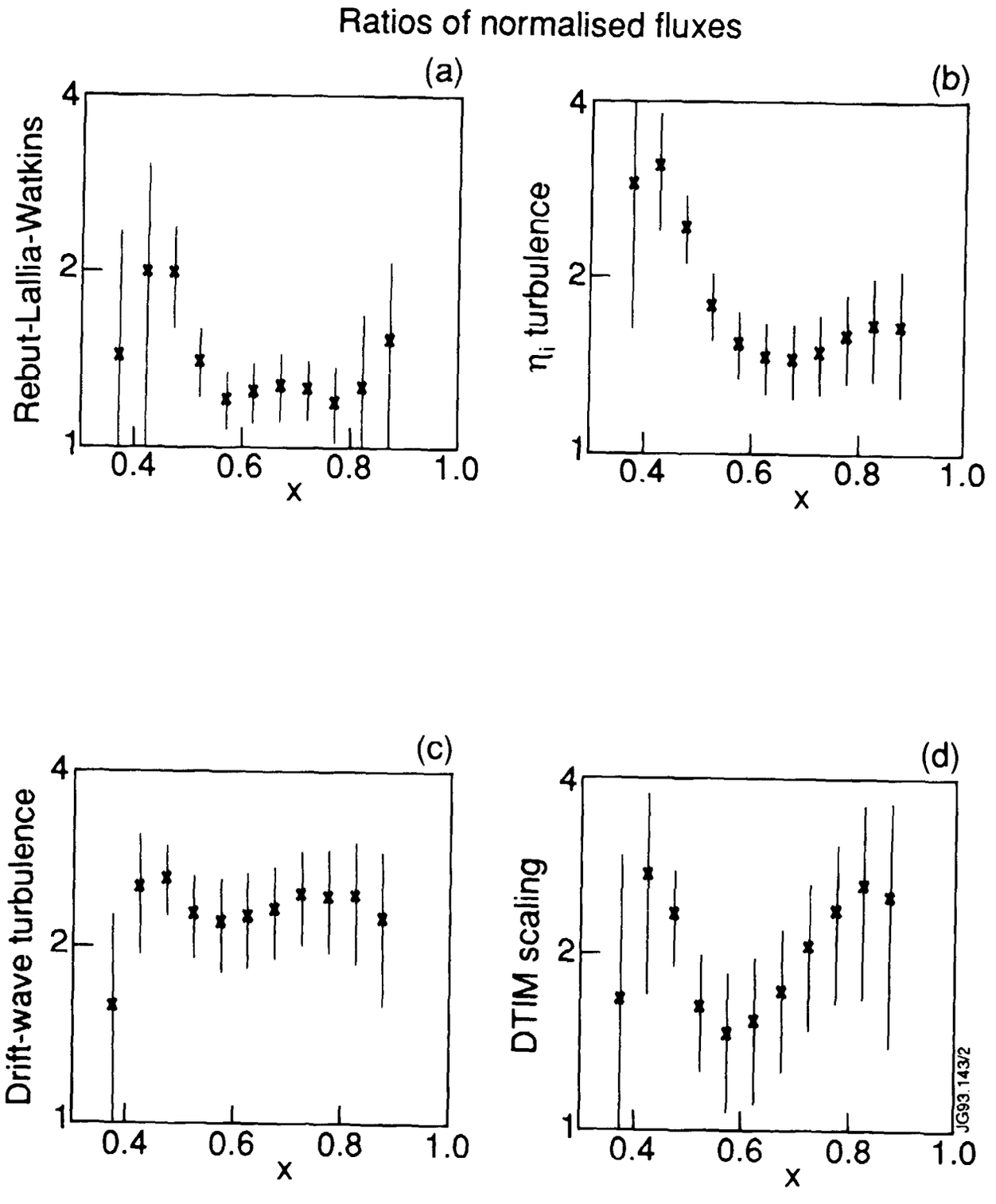

Fig. 7: As Fig. 6 but with F given by the scalings of (a) Rebut-Lallia-Watkins, (b) η_i-modes, (c) drift waves, (d) DTIM.

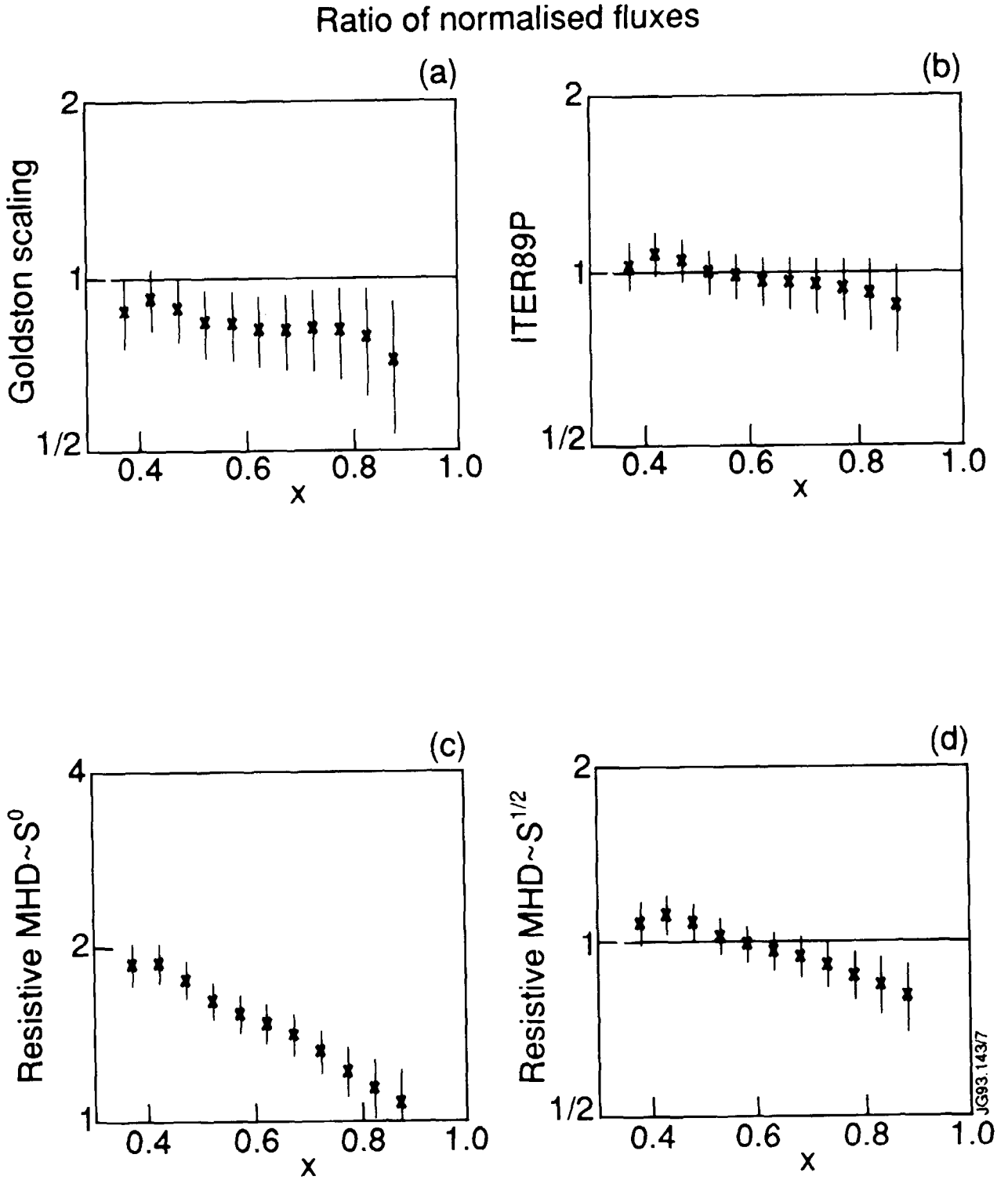

Fig. 8: As Figs. 6 and 7 but with F given by scalings of (a) Goldston scaling, (b) ITER89P, (c) resistive MHD ~ S^0, (d) resistive MHD ~ $S^{1/2}$.

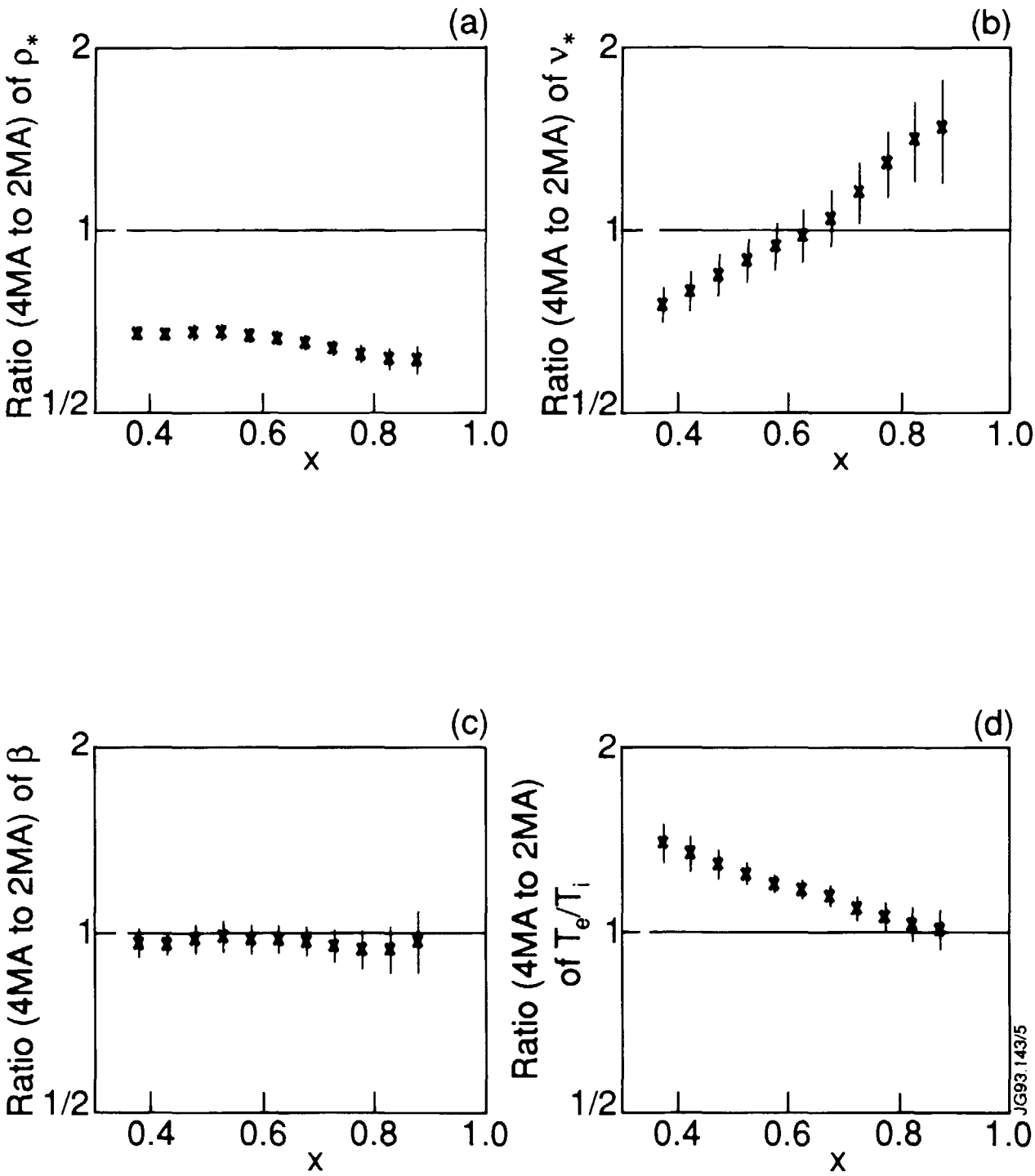
(a)
Ratio (4MA to 2MA) of ρ*
2
1
1/2
0.4
0.6
0.8
1.0
x
(b)
Ratio (4MA to 2MA) of ν*
2
1
1/2
0.4
0.6
0.8
1.0
x
(c)
Ratio (4MA to 2MA) of β
2
1
1/2
0.4
0.6
0.8
1.0
x
(d)
Ratio (4MA to 2MA) of T_e/T_i
2
1
1/2
0.4
0.6
0.8
1.0
x
JG93.143/5